Catalysis Today 144 (2009) 31–36

Contents lists available at ScienceDirect

Catalysis Today

journal homepage: www.elsevier.com/locate/cattod

N-doped TiO_2 from $TiCl_3$ for photodegradation of air pollutants

Claudia L. Bianchi [a,b,*], Giuseppe Cappelletti [a,b], Silvia Ardizzone [a,b], Stefano Gialanella [c], Alberto Naldoni [a], Cesare Oliva [a], Carlo Pirola [a]

[a] Department of Physical Chemistry and Electrochemistry, University of Milan, Via Golgi 19, 20133 Milano, Italy
[b] Consorzio INSTM, Via Giusti 9, 50121 Firenze, Italy
[c] Department of Materials Engineering and Industrial Technologies, University of Trento, 38050 Mesiano (TN), Italy

ARTICLE INFO

Article history:
Available online 29 January 2009

Keywords:
N-doped TiO_2
Photocatalytic activity
Visible light
EPR
XPS

ABSTRACT

The photocatalytic activity of both commercial and homemade N-doped TiO_2 samples, prepared at different pH from $TiCl_3$ solutions, was tested for the degradation of toluene in the gas phase by using a solar irradiation source. Highest degradations and corresponding kinetic constants were achieved in the case of N-doped samples prepared at higher pH.

Various adsorbed aromatic species (benzoic acid, the major surface product, benzylic alcohol, benzaldehyde) were observed at the surface of the exhaust catalysts by using FTIR-ATR spectroscopy. The trend of the photocatalytic efficiency in the visible region is discussed with respect to structural (XRD), morphological (BET, TEM), surface (XPS) and paramagnetic (EPR) characterization.

1. Introduction

Photocatalysis is raising much attention owing to its potential applications in environmental remediation, the photo-electrochemical splitting of water and the conversion of solar energy to electric power. TiO_2 is the most frequently employed photocatalyst owing to its cheapness, non-toxicity, and structural stability [1,2]. To date, a great number of attempts have been made to promote the practical photocatalytic applications of TiO_2 by extending the spectral response from the UV area to the visible region and enhancing quantum efficiency. The doping of TiO_2 with non-metal ions has raised recently an enormous interest especially in the case of nitrogen-doped samples [3–13]. The biggest advantage of N-doped TiO_2 samples, compared to pure TiO_2, is their lower excitation energy, which not only allows the absorbance of the UV portion of solar light, but also of the visible portion, which covers >50% of the solar energy.

Several points are still open to debate in the understanding of N-doped samples behaviour. One of the main debated questions concerns the electronic structure of these systems, i.e. whether the enhanced visible-light absorbance is due to a narrowed band gap or mainly to the introduction of localized impurity states in the band gap. Further questions regard the actual localization of N species in the TiO_2 lattice either interstitial or substitutional and their interactions with oxygen vacancies [3–13].

Different methods are presented in the literature to incorporate nitrogen in titanium dioxide, and different sources of N are adopted (NH_3/NH_4^+, amines, nitrides, etc.) [7–14]. The different synthetic procedures may lead to materials showing even significantly different properties.

In this work TiO_2 samples were prepared through a composite route starting from strongly acid $TiCl_3$ aqueous solutions. N species are loaded by NH_3 in the liquid phase. A final calcination step at mild temperatures promotes the crystallization of the amorphous precursors. The synthetic reaction implies an accurate control of the suspension pH during the formation of the TiO_2 precursors.

The structure, morphology and chemical composition of the nitrogen-doped sub-surface region are investigated by X-ray diffraction, TEM and XPS. Moreover, EPR spectra are obtained to characterize paramagnetic centres. The doping effect on the photoactivity is measured in the case of the photodegradation of toluene; the nature of the surface species adsorbed onto exhaust catalysts is investigated by FTIR-ATR in order to evaluate the progress of the oxidation reaction.

2. Experimental

2.1. Sample preparation

All the chemicals were of reagent grade purity and were used without further purification; doubly distilled water passed through a Milli-Q apparatus was used to prepare solutions and suspensions.

* Corresponding author at: Department of Physical Chemistry and Electrochemistry, University of Milan, Via Golgi 19, 20133 Milano, Italy. Tel.: +39 0250314253; fax: +39 0250314300.
E-mail address: claudia.bianchi@unimi.it (C.L. Bianchi).

0920-5861/$ – see front matter © 2008 Elsevier B.V. All rights reserved.
doi:10.1016/j.cattod.2008.12.019

N-doped samples were obtained starting from a $TiCl_3$ salt solution (12% in hydrochloric acid) by successive addition of ammonia solutions at different concentrations (2, 4 and 6 M) in order to achieve pH 4 (TN4), 7 (TN7) and 9 (TN9), and with a starting N/Ti molar ratio of 6.6, 7.6 and 9.2, respectively. The mixture was kept stirred under O_2 stream (10 nL/h) till the disappearance of the blue colour of the slurry (about 5 h) due to the oxidation of $Ti(OH)_3$. The wet precursors were dried in oven at 80 °C overnight and subsequently calcined at 300 °C for 6 h. Then the calcined powders were washed with a solution of ethanol/water (80:20) to eliminate the salt, reaching conductivity values in the washing solutions of about 1 mS. The undoped reference sample (T9) was obtained by the same procedure at pH 9, using KOH instead of ammonia.

Homemade powders were compared with different commercial samples: A_287 (Alfa Aesar), PC105 (Millennium Inorganic Chemicals), P25 (Degussa) and NanoActive (NanoScale Corporation).

2.2. Sample characterization

Room-temperature X-ray powder diffraction (XRPD) patterns were collected between 20° and 90° with a Siemens D500 diffractometer, using Cu Kα radiation. For all studied samples, powder patterns were collected with a counting time of 20 s for each a 0.08° step. Rietveld refinement has been performed using the GSAS software suite and its graphical interface EXPGUI [15]. The average diameter of the crystallites, *d*, was estimated from the most intense reflection (1 0 1) of the TiO_2 anatase phase using the Scherrer equation [16].

Specific surface areas were determined by the classical BET procedure using a Coulter SA 3100 apparatus.

Diffuse reflectance spectra of the powders were measured on UV–vis scanning spectrophotometer (PerkinElmer, Lambda 35), which was equipped with a diffuse reflectance accessory, as reported previously [2].

X-ray photoelectron spectra were taken in an M-probe apparatus (Surface Science Instruments). The source was monochromatic Al Kα radiation (1486.6 eV) as in reference [17].

EPR spectra have been collected at room temperature by means of a Bruker Elexsys spectrometer at the working frequency of *ca.* 9.4 GHz. The spectral simulations were obtained by the Bruker SimFonia programme.

Transmission electron microscopy (TEM) observations were conducted at 120 keV using an analytical microscope equipped with an energy dispersive X-ray spectrometer (EDXS). The powder samples were ultrasonically suspended in alcohol and then spread onto a copper grid covered with an amorphous carbon film.

2.3. Photocatalytic experiments

Photocatalytic degradations of toluene were conducted in a Pyrex glass cylindrical reactor with diameter of 200 mm and effective volume of 5 L, as already described [18]. The gaseous mixture in the reactor was obtained by mixing hot chromatographic air, humidified at 60%, and the fixed amount of volatilized (250 °C) toluene, in order to avoid condensation. The initial concentration of toluene in the reactor was 500 ppm. Photon source was provided by a 300 W solar lamp (Radium Sanolux HRC 300-280) emitting in the 380–600 nm wavelength range (radiation intensity of $I = 1.2 \times 10^{-5}$ Einstein dm^{-3} s^{-1}).

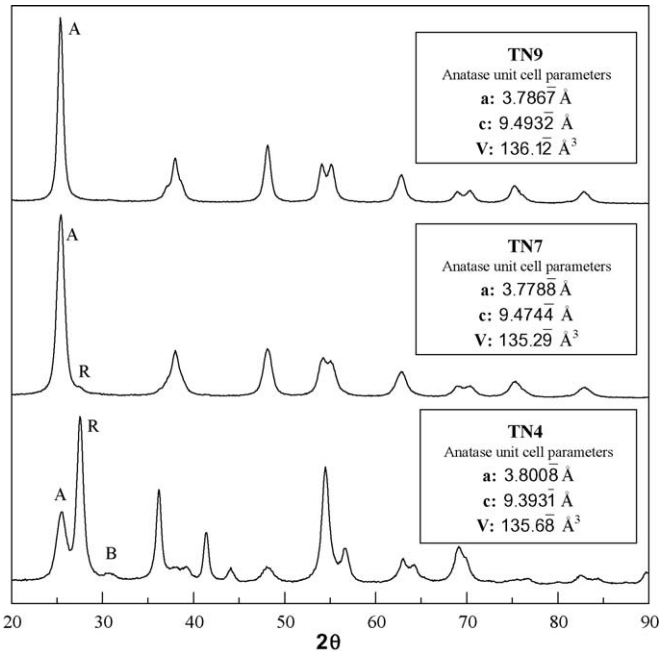

Fig. 1. Powder X-ray diffraction lines and relative anatase cell parameters of TN4, TN7 and TN9 samples (A = anatase, B = brookite and R = rutile). Theoretical anatase unit cell parameters: *a*, *b* = 3.7845 Å, *c* = 9.5143 Å and *V* = 136.27 Å^3.

3. Results and discussion

3.1. Structural and morphological characterization

Fig. 1 reports the X-ray diffractograms of the three, nitrogen doped, samples prepared starting from $TiCl_3$, at different pH values. By analyzing the features of the diffractograms, it can be immediately observed that pH plays a key role in imposing the sample phase composition, in terms of relative enrichment in the three TiO_2 polymorphs. The phase composition of the various samples, obtained by the Rietveld method, is reported in Table 1. At pH 4 rutile is the prevailing phase, although also anatase and brookite are present as minor components. In the presence of chlorides and at acid pH the formation of nanocrystalline rutile is reported to be promoted [2]. At neutral pH, anatase is the main component in the presence of traces of rutile, while only at pH 9 the pure anatase phase can be obtained. In the case of the sample obtained at pH 9 in the absence of N species (T9), the pattern of the

Table 1
Quantitative phase composition (A = anatase, B = brookite, R = rutile), crystallite anatase and rutile diameter by XRD (Scherrer equation), BET surface area; total pore volume, N/Ti by XPS analysis.

Sample	%A	%B	%R	d_A^{101} (nm)	d_R^{110} (nm)	S_{BET} (m^2 g^{-1})	V_{pore} (ml g^{-1})	N/Ti
T9	–	–	–	–	–	2	0.014	–
TN4	14	11	75	–	11 ± 2	103	0.355	0.016
TN7	97	–	3	9 ± 1	–	97	0.356	0.037
TN9	100	–	–	11 ± 2	–	102	0.439	0.028
NanoActive	–	–	–	–	–	>500	>0.400	–
A_287	100	–	–	9 ± 1	–	287	0.442	–
PC105	100	–	–	20 ± 4	–	73	0.384	–
P25	80	–	20	25 ± 5	35 ± 8	50	0.256	–

diffractogram (not reported for reasons of space) shows that the sample, although calcined at the same temperature of the samples containing N species, is still amorphous. Due to the presence of the large amount of KCl coprecipitated with the oxide the specific surface area and pore volume appear to be very low (Table 1, columns 7,8). Apparently the presence of N species promotes crystallization in otherwise identical conditions. The anatase unit cell parameters obtained by the Rietveld refinement are reported in Fig. 1 for each sample. Parameters pertaining to the sample obtained at pH 9 match closely the theoretical values while in the case of the sample obtained at pH 7 an appreciable shrinking of the unit cell volume is observed. Di Valentin et al. [6], on the grounds of DFT calculations, report slightly longer Ti–N bond lengths (1.964 and 2.081 Å) with respect to Ti–O ones (1.942 and 2.002 Å). Experimental data on the effects of N-doping on unit cell parameters of anatase are very scanty in the literature. The only pertinent result is that by Song et al. [19] reporting "slightly smaller" lattice parameters of N-doped samples with respect to pure TiO_2. The present lattice parameters of TN7 might suggest, also on the grounds of XPS data presented in the following, a location, at least in part, substitutional for N species in the TiO_2 lattice in the case of this sample. The minority presence of anatase in sample TN4 does not allow straightforward conclusions to be drawn in the case of this sample. Table 1 reports the crystallite size obtained by elaboration of the most intense diffraction peak by the Scherrer's equation. The modulation of pH, although relevantly affecting the phase composition, does not significantly modify either the crystallite size or the specific surface area. Further, the values of specific surface areas show, when compared with the crystallite sizes, the occurrence of a relevant degree of aggregation between the crystallites in the actual particles. Table 1 reports also results of characterizations of commercial TiO_2 samples to be used as reference systems in the analysis of the photodegradation results.

3.2. TEM characterization

TN4 (Fig. 2) displays well-crystallised grains with size ranging from 10 nm up to 30 nm approximately. The grains show quite different morphologies: from round shaped to prismatic, although in all cases rather isotropic. The relevant diffraction pattern (inset) displays the presence of the characteristic lines of all three polymorphs of the titanium oxide, in agreement with the XRD results. In the case of TN7 the observed microstructure shows mostly equiaxed domains with an average size close to 10 nm, in agreement with the predictions of XRD analyses, as concerns anatase. The other expected polymorph (rutile) has not been detected, since, as indicated by the XRD results, its concentration is too low. The typical grain morphology of TN9 is shown in the figure, where the mostly equiaxed grains of the powder have size ranging from a few nanometres up to 30 nm or so. In this respect the grain size distribution looks comparatively broader than in the former sample (TN7). The corresponding SAED pattern (inset) confirms the presence, as the only phase in this material, of the anatase polymorph.

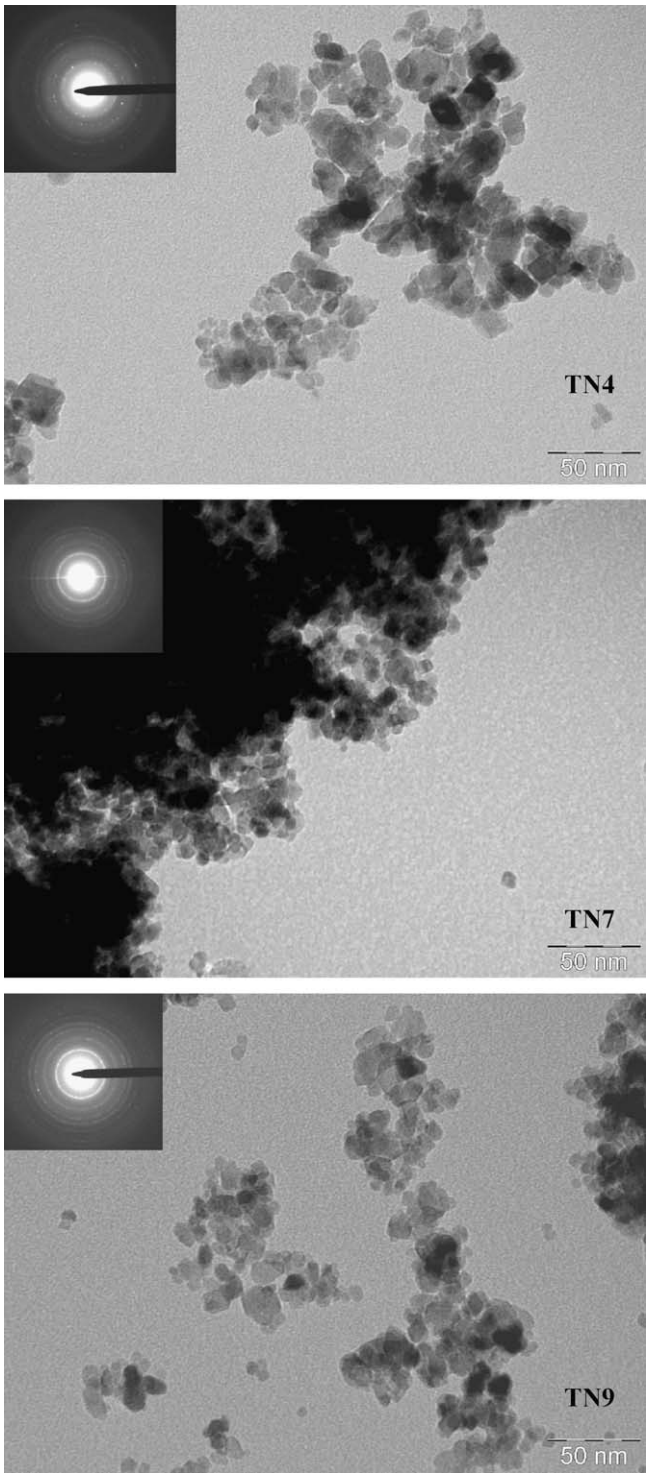

Fig. 2. TEM images and the relevant SAED pattern (inset) for TN4, TN7 and TN9 samples.

3.3. Optical absorption

Fig. 3 reports the comparison among the diffuse reflectance (DR)UV–vis spectra of N-doped TiO_2 prepared from $TiCl_3$, of the reference sample T9 and of an un-doped commercial pure anatase sample. The curve relative to TN9 essentially differs from that of bare TiO_2 for the broad absorption in the visible region centred at about 450 nm, in analogy with what reported by other authors for N-doped TiO_2 [6,7]. The spectra relative to TN7 and TN4 show increased absorption in the visible region, the more so in the case of the sample prepared at pH 4. This effect is to be related, besides to the presence of N species, also to the absorption in the visible region typical of rutile, which is present in these samples, reaching 75% of the phase abundance in the case of the TN4.

3.4. XPS analyses

Table 1 reports the N/Ti atomic ratios obtained by XPS on the present N-doped samples. The trend is not monotonically varying with pH, the sample showing the largest N content is the sample

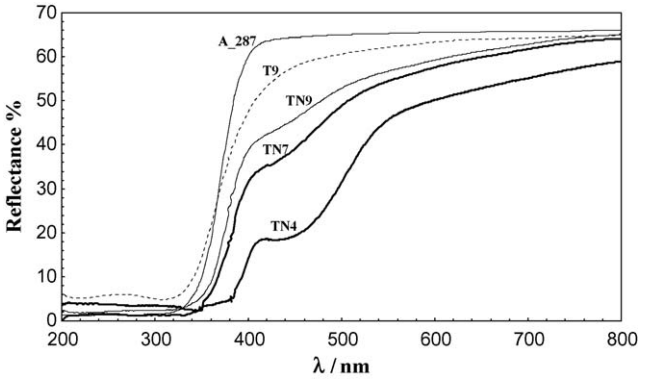

Fig. 3. Diffuse reflectance spectra for commercial (A_287) and homemade (T9, TN4, TN7 and TN9) samples.

obtained at intermediate pH (TN7). The sample obtained at pH 4 shows the lowest N content and a broad N 1s peak which is difficult to fit. The N 1s region of the two samples obtained respectively at pH 7 and 9 is instead more defined and is reported in Fig. 4. It can be observed that the fitting procedure allows in the case of TN9 the identification of only one component centred at 400.1 eV while in the case of sample TN7 two components respectively at 396.1 and 399.9 eV are clearly appreciable. The debate on the attribution of XPS N 1s peak components to specific species or structures (O–Ti–N, N–O–Ti–O or O–N–Ti–O, etc.) is definitely open and well discussed in Ref. [20]. XPS N 1s peaks in the range (396–404 eV) were observed by several authors and generally peaks at 396–397 eV were attributed to substitutional nitrogen while peaks at higher binding energies (e.g. 400 eV) were attributed to interstitial locations. In the present case the attribution of the component at 396.1 eV to substitutional N, in the case of sample TN7, could be supported by the values of the cell parameters obtained by elaboration of XRD data. Just in the case of this sample the cell parameters show appreciable shrinking with respect to both theoretical and experimental values obtained for the samples prepared at different pH. In the case of sample TN9 a sole interstitial location of N species could be proposed also on the grounds of the almost un-modified cell parameters. The convergence between XPS and XRD data suggests, in the case of the present samples, a homogeneous distribution of N species between particle surface/sub-surface and bulk. It is interesting to recall that in the case of TiO_2 prepared by a sol-reaction and N doped by different inorganic compounds, Di Valentin et al. [11] never observed peaks at 396 eV. Again, therefore, the specific conditions of the TiO_2 preparative reactions are found to play a key role on the features of the N-doped samples.

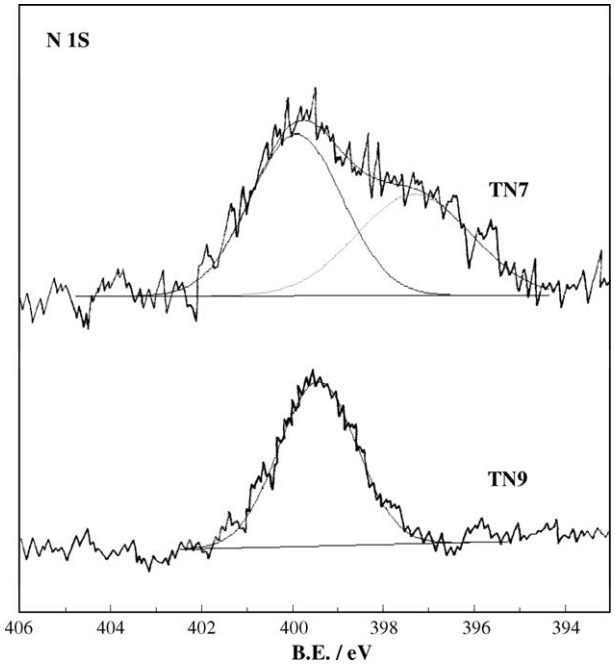

Fig. 4. XPS spectra: N 1s region for TN7 and TN9 samples.

3.5. EPR results

The most intense EPR feature has nearly the same shape for the three N-doped samples with relative intensities respectively of 1:2.1:2.9 for TN4, TN7 and TN9. The large width of the lines employed in the spectral simulation in the *xy* plane could suggest the presence of either unresolved interactions with N nuclei or that of many different coordinative environments around each paramagnetic centre. These spectra are rather similar to those elsewhere attributed to NO with the unpaired electron confined in the 2π antibonding orbital with lower energy [8]. However in that case the spectrum was observable only at $T < 170$ K and interactions with N nuclei were also determined. Similar spectra were also reported for N-doped TiO_2 photocatalysts [9] and attributed to the overlapping contributions of Ti^{3+} "trapped electrons" and of $O^{-\bullet}$ "trapped holes" [21]. Indeed, both these species would form with $TiO_{2-x}N_x$ [10,22]. Ti^{3+} ions are characterized by very short relaxation time, so that their EPR spectrum is observable at very low temperature only or, at room temperature, with Ti^{4+} coupled with species like $O^{-\bullet}$ [22,23]. In any case it can be noted that the last interpretation, as well as that based on the presence of NO, would indicate an increasing amount of N doping with increasing pH.

Furthermore, in the present case, a second EPR component is appreciable, the intensity increasing in the order TN4 < TN7 < TN9. Fig. 5 and inset show, as an example, the spectrum obtained by subtracting TN7 from TN9 spectrum. This difference spectrum (Fig. 5, inset) is composed by three lines due to an unpaired electron interacting with a nuclear spin $I = 1$, and can be univocally attributed to $N_b^{\bullet}$ centres formed by an unpaired 2p electron belonging to an (interstitial or substitutional) N atom [7,8,11]. Systems of this kind are typical of N–TiO_2 submitted to oxidation [7] and are of great interest for visible-light absorption [7]. Furthermore, their importance resides also in the fact that their presence would reduce from 4.2 to 0.6 eV the cost of V_0 formation in bulk TiO_2 [7,11]. All these EPR patterns are not observable with the T9 sample (TiO_2 without N radicals), which displays only a less intense EPR pattern centred approximately at $g \cong 2.003$ (Fig. 5(d)).

3.6. Photocatalytic activity

For all the present TiO_2 samples the photocatalytic activity was tested with respect to the degradation of toluene. The reaction

Table 2
Photocatalytic % degradation, pseudo-first-order kinetic constant together with relative standard deviation and regression coefficient for all samples (n.d. = not determined).

Sample	%Degradation	κ ($\times 10^3$ min^{-1})	R^2
T9	13.7	0.6 ± 0.3	0.980
TN4	56.2	2.9 ± 0.1	0.991
TN7	65.0	4.2 ± 0.1	0.987
TN9	79.6	6.0 ± 0.2	0.990
NanoActive	35.2	1.0 ± 0.3	0.991
A_287	55.8	n.d.	–
PC105	47.7	n.d.	–
P25	56.0	n.d.	–

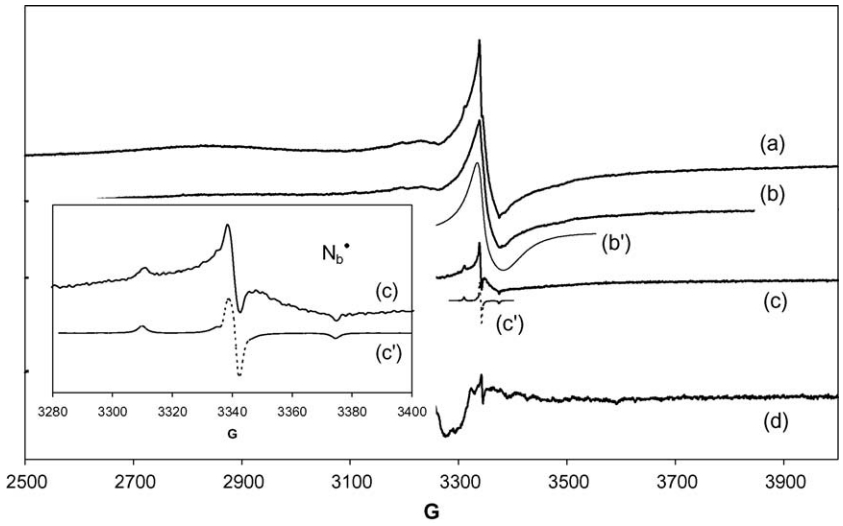

Fig. 5. EPR spectra obtained at room temperature with (a) TN9, (b) TN7 and (d) T9 samples, respectively. The difference between tracks (a) and (b) multiplied by 1.38 gives (c). (b′) is the simulation of (b) with $g_x \approx 1.978$; $g_y \approx 1.993$; $g_z \approx 2.003$ (i.e. $\langle g \rangle \cong 1.99$) and Lorentzian-component lines with peak-to-peak widths $\Delta H_{pp} \cong 60$; 60; 12 G along the *x*, *y*, *z* axis, respectively. (c′) is the simulation of (c) with $g_x \approx 2.005$; $g_y \approx 2.004$; $g_z \approx 2.003$ and $A_z = 32.3$ G.

kinetics can be described for all the synthesized samples by a pseudo-first-order rate equation. The rate constant (κ) values for the different catalysts, evaluated by linear fitting of the logarithmic plot of the residual toluene amounts (determined by GC) as a function of the reaction time, are listed in Table 2. In the case of three of the commercial samples elaboration by a pseudo-first-order rate equation did not yield significant results as observed previously in the case of P25 [18].

Fig. 6 reports the trend of percent degradation of toluene, in humid conditions, for the present TiO_2 photocatalysts. It can be immediately observed that the sequence in the final degradation follows the same order of the rate constants reported in Table 2. The commercial samples, not promoted by N species, both the pure anatase (A_287 and PC105) and the mixed phase P25, show relatively low efficiencies with respect to N-doped ones. An increase in the photocatalytic activity for N-doped samples has been reported for different photocatalytic reactions [24]. Livraghi et al. [7], for example, report that the activity of N–TiO_2 in the photodegradation of methylene blue is definitely although not largely higher than that of the bare oxide.

The three N-doped samples obtained from $TiCl_3$, show increasing conversion with increasing the pH of the synthetic reaction. The sample obtained at pH 9 shows a top conversion reaching a degradation of around 80% after 280 min reaction time and showing the largest rate constant.

FTIR-ATR spectra of TN7 and TN9 withdrawn at the end of the toluene degradation reaction are reported in Fig. 6 (inset). For each catalyst the "blank" curve pertaining the pure oxide was subtracted. In the figure only few of the most intense bands are evidenced for the sake of clarity [18]. The two spectra show the presence of several common bands (toluene, benzoic acid, benzaldehyde and benzyl alcohol), but with different relative

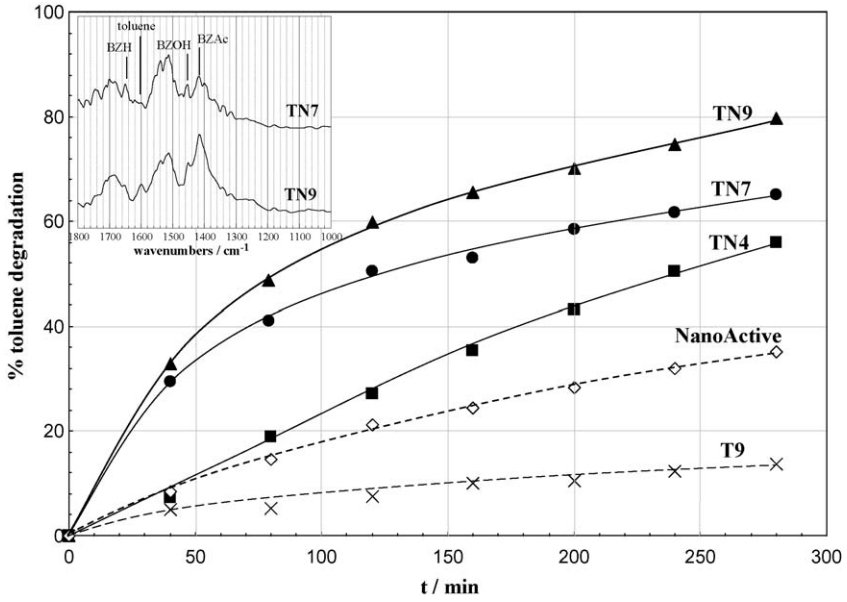

Fig. 6. Toluene photodegradation for amorphous (T9 and NanoActive) and crystalline (TN4, TN7 and TN9) samples. Inset: IR spectra of TN7 and TN9 sampled at the end of the photocatalytic run. For each oxide, the curve of the relative pure TiO_2 was subtracted. Only the major (or most appreciable) bands of the adsorbed species are evidenced (see Ref. [18]).

intensities. In the case of sample TN9, in agreement with the faster kinetics (sample TN9, $\kappa = 6.0 \times 10^{-3}\,min^{-1}$; sample TN7, $\kappa = 4.2 \times 10^{-3}\,min^{-1}$, see Table 2), the BZAc (benzoic acid) component appears the most abundant adsorbed species with respect to TN7, showing a more advanced oxidation reaction. In fact the degradation sequence implies the progressive degradation from toluene to benzoic acid species, passing through benzylic alcohol and benzaldehyde.

It is interesting to observe that the sequence in degradation, among the $TiCl_3$ samples, does not match the sequence in optical absorption reported in Fig. 3. Since the present three N-doped samples show fully comparable surface areas and crystallite sizes effects different from morphology or microstructure have to be invoked to interpret the observed trend.

No systematic results could be found in the literature concerning the role played by the TiO_2 polymorph hosting N species on the photocatalytic efficiency of TiO_2 by solar irradiation. Data by model representation show that rutile and anatase accommodate differently N species [6]. No results could be found concerning brookite. Results in Fig. 6 may indicate that pure anatase hosting N species is more active than a mixture of anatase and rutile. Further the comparison between the activity of samples TN7 and TN9 may suggest that substitutional N sites yield less active photocatalysts than interstitial ones. Data in the literature are controversial on this point. Di Valentin et al. [6], in the case of films prepared by chemical vapour deposition observed no evidence of photocatalytic activity in the visible in the case of N substitutional sites. Asahi et al. [3], instead, in the case of powdered samples prepared with NH_3/Ar as the source of N attributed visible photoactivity to substitutional sites associated with an XPS peak at 396 eV.

The sequence in photocatalytic activity seems to correlate simply with EPR results which show an increasing amount of paramagnetic centres with increasing the reaction pH, the sample prepared at pH 9 containing an additional amount of paramagnetic N centres even with respect to sample TN7.

4. Conclusions

The first aspect which can be commented regards the role played by the pH of the synthetic reaction on the features of the obtained photocatalysts. Actually pH intervenes in modifying all the investigated features of the material, including the photocatalytic activity. The photoactivity with respect to toluene degradation follows the order of increasing pH; this sequence does not match either the trend shown by XPS for the surface/subsurface N amount or the possible presence of substitutional N in the TiO_2 lattice. The origin of the best performance of TN9 is to be sought in the largest amount of paramagnetic centres present in this sample as reported by EPR results.

Acknowledgments

Part of the research has been financed by the Project DIGITEM, sponsored by the Provincia Autonoma di Trento. This research has been supported by the University of Milan Research Funds (FIRST, PUR).

References

[1] M. Anpo, Bull. Chem. Soc. Jpn. 77 (2004) 1427.
[2] G. Cappelletti, C.L. Bianchi, S. Ardizzone, Appl. Catal. B: Environ. 78 (2008) 193.
[3] R. Asahi, T. Morikawa, T. Ohwaki, K. Aoki, Y. Taga, Science 293 (2001) 269.
[4] Y. Huo, Z. Bian, X. Zhang, Y. Jin, J. Zhu, H. Li, J. Phys. Chem. C 112 (2008) 6546.
[5] A.V. Emeline, G.N. Kuzmin, N. Serpone, Chem. Phys. Lett. 454 (2008) 279.
[6] C. Di Valentin, E. Finazzi, G. Pacchioni, A. Selloni, S. Livraghi, M.C. Paganini, E. Giamello, Chem. Phys. 339 (2007) 44.
[7] S. Livraghi, M.C. Paganini, E. Giamello, A. Selloni, C. Di Valentin, G. Pacchioni, J. Am. Chem. Soc. 128 (2006) 15666.
[8] S. Livraghi, A. Votta, M.C. Paganini, E. Giamello, Chem. Commun. (2005) 498.
[9] S.K. Joung, T. Amemiya, M. Murabayashi, K. Itoh, Appl. Catal. A: Gen. 312 (2006) 20.
[10] N. Serpone, J. Phys. Chem. B 110 (2006) 24287.
[11] C. Di Valentin, G. Pacchioni, A. Selloni, S. Livraghi, E. Giamello, J. Phys. Chem. B 109 (2005) 11414.
[12] S. Sakthivel, M. Janczarek, H. Kisch, J. Phys. Chem. B 108 (2004) 19384.
[13] S. Sato, R. Nakamura, S. Abe, Appl. Catal. B 284 (2005) 131.
[14] T. Morikawa, R. Asahi, T. Ohwaki, K. Aoki, Y. Taga, Jpn. J. Appl. Phys. 40 (2001) L561.
[15] A.C. Larson, R.B. Von Dreele, GSAS: General Structural Analysis System, Los Alamos National Laboratory, Los Alamos, NM, 1994.
[16] S. Ardizzone, C.L. Bianchi, G. Cappelletti, S. Gialanella, C. Pirola, V. Ragaini, J. Phys. Chem. C 111 (2007) 13222.
[17] G. Cappelletti, C.L. Bianchi, S. Ardizzone, Appl. Surf. Sci. 253 (2006) 519.
[18] S. Ardizzone, C.L. Bianchi, G. Cappelletti, A. Naldoni, C. Pirola, Environ. Sci. Technol. 42 (2008) 6671.
[19] K. Song, J. Zhou, J. Bao, Y. Feng, J. Am. Ceram. Soc. 91 (2008) 1369.
[20] A.V. Emeline, V.N. Kuznetsov, V.K. Rybchuk, N. Serpone, Int. J. Photoener. (2008), doi:10.1155/2008/258394.
[21] J.E. Wertz, J.R. Bolton, Electron Spin Resonance. Elementary Theory and Applications, McGraw-Hill, 1972, p. 317.
[22] R.F. Howe, M. Grätzel, J. Phys. Chem. 89 (1985) 4495.
[23] C. Oliva, L. Bonoldi, S. Cappelli, L. Fabbrini, I. Rossetti, L. Forni, J. Mol. Catal. A: Chem. 226 (2005) 33.
[24] J.L. Gole, J.D. Stout, C. Burda, Y. Lou, X. Chen, J. Phys. Chem. B 108 (2004) 1230.